Journal of Materials Chemistry A

Accepted Manuscript

ROYAL SOCIETY OF CHEMISTRY

www.rsc.org/materialsA

Journal of
Materials Chemistry A

Cite this: DOI: 10.1039/c0xx00000x

ARTICLE TYPE

www.rsc.org/xxxxxx

Magnetic molecularly imprinted microsensor for selective recognition and transport of fluorescent phycocyanin in seawater

Zhong Zhang,[ab] Jinhua Li,[a] Longwen Fu[a], Dongyan Liu[a] and Lingxin Chen*[a]

Received (in XXX, XXX) Xth XXXXXXXXX 20XX, Accepted Xth XXXXXXXXX 20XX
DOI: 10.1039/b000000x

Phycocyanin with excellent fluorescent characteristics and important physiological significance is an effective indicator for cyanobacterial bloom assessment due to its close relationship with cyanobacteria biomass. Molecularly imprinted polymers (MIPs) have aroused great interest owing to its recognition specificity; micromotor-driven targeted transport capability holds considerable promise. Herein, we proposed an attractive magnetic microsensor for selective recognition, enrichment and transport of label-free fluorescent phycocyanin by combining MIPs and catalytic micromotor. The MIP-based catalytic microsensor was fabricated using phycocyanin as imprinting molecule, Ni (0.55%) as magnetic navigation material, and Pt (24.55%) as solid support/catalyst to facilitate freely moving in solutions, as well as additional magnetic field was employed for trajectory control. The autonomous self-propulsion microsensor vividly displayed their motion states, presenting two different trajectories. The movement velocity was well calculated based on the body-deformation model, suggesting a linear positive correlation between the velocity and hydrogen peroxide concentration, with a high average speed of 163 μm/s. In addition, high efficient targeted identification and enrichment abilities were demonstrated based on the magnetic imprinted layer. More excitingly, no obvious interference was found from complicated matrices such as seawater samples, along with a real-time visualization of the phycocyanin loading and transport. The sensing strategy would not only provide potential applications for rapid microscale monitoring of algae blooms, but also enrich the research connotations of protein imprinting.

1. Introduction

Cyanobacterial blooms are one of the major adverse events for inland waters because of the eutrophication processes induced by urbanization, industrial and agricultural activities.[1] Phycocyanin, a blue colored photosynthetic accessory pigment protein, displays important biological significance,[2] and is also an effective indicator for the cyanobacterial bloom assessment due to its close relationship with cyanobacteria biomass.[3] Hence, recognition, determination and removal of phycocyanin is being increasingly investigated since the monitoring and remediation of cyanobacterial blooms has become a crucial global issue.[4,5] Phycocyanin emits fluorescence at about 615–640 nm, has high absorption coefficient in a wider spectral range, and is stable in water for a long time. So, the protein has become a new desirable fluorescent marker with high stability and sensitivity and can be applied in many aspects especially life, biomedical and environmental fields.[6,7] Therefore, we also aspire to perform related fluorescent sensing studies on phycocyanin.

Molecular imprinting technology has aroused great interest owing to its unique properties of structure predictability, recognition specificity and application universality, and the features have been displayed by molecularly imprinted polymers (MIPs).[8–10] Recently, MIPs on the surface of matrices have displayed excellent perspectives especially for protein imprinting.[9,11] Compared to traditional MIPs, surface imprinting polymers have some special advantages such as more complete template removal, better site accessibility and lower mass transfer resistance, and thereby higher selective enrichment ability.[12–14]

In recent years, catalytic micro/nanomotors have gotten bigger developments in motion control, in which magnetic materials can generally be used to control the movement and achieve a predetermined path.[15,16] So, excitedly, the coupling of surface imprinting and micro/nanomotors preparation technologies can provide tailor-made self-propelled micro/nanomotors with predetermined specificities for selective capture and transport of targets. Compared to traditional biological molecular motors, the present synthesis and preparation processes of imprinted catalytic micro/nanomotors are simpler, controllable and longer working lives, have good reproducibility and low environmental requirements, and facilitate functionalization and integration.[17] Besides, the recognition properties of the synthetic imprinted micro/nanomotors can withstand harsher conditions than their natural counterparts, which make the MIP-based

micro/nanomotors especially attractive for diverse practical applications. In addition, hydrogen peroxide fuel can affect the stability and recognition properties of biological molecular motors, but it has almost no effect on the MIP ones.[18] However, to the best of our knowledge, few work combining micromotors and molecular imprinting has been reported.[19] Accordingly, we expect to construct a new simple MIP-based label-free fluorescent micromotor sensor that can recognize and transport some special proteins, such as the phycocyanin.

Herein, we develop a simple, magnetic surface-imprinted micromotor fluorescent sensor using integration of molecular imprinting and catalytic micromotor for convenient, rapid and sensitive recognition and transport of phycocyanin in seawater. Phycocyanin is selected as imprinting molecule and label-free fluorescent marker, and hydrogen peroxide for catalytic propulsion. The present microsensor mainly profits from the following advantages: i) simple preparation, without involving chemical reactions or harsh conditions, ii) excellent control of the polymerization and localization of the microstructures by electrosynthesis, iii) the specific electrosensing polymeric material exhibits 3D microstructures and superior resistance against nonspecific protein adsorption, and finally provides good binding capacity and sensitivity, and iv) it is reasonable to expect that the system is scalable down to the nanosize. The microsensor is fully characterized by SEM, EDX mapping samples, fluorescence spectroscopy/microscopy and confocal laser scanning microscope. The motion control capacity and fluorescent detectability are investigated in detail. Moreover, the magnetic imprinted microsensor is successfully applied to complex seawater sample analysis and provides satisfactory real-time visualization of the phycocyanin loading and transport.

2. Experimental

2.1 Reagents and materials

Phycocyanin was kindly provided by Shandong Oriental Ocean Company (Yantai, China) and used as the template protein. Bovine serum albumin (BSA), 3,4-ethylenedioxythiophene (EDOT), poly(sodium-4-styrenesulfonate) (NaPSS, MW~70 000), sodium cholate, nickel aminosulfonate ($Ni(H_2NSO_3)_2{\cdot}4H_2O$), and sodium dodecyl sulfate (SDS, MW 288.38 g/mol), were purchased from Sigma-Aldrich (Shanghai, China). Hydrogen peroxide (H_2O_2), chloroplatinic acid (H_2PtCl_6), lead nitrate ($Pb(NO_3)_2$), hydrochloric acid (HCl), ethanol, Tween-20, boron hydrogen acid (H_3BO_3), dichloromethane, nickel chloride, potassium chloride and other affiliated chemicals were all obtained from Sinopharm Chemical Reagent Co. Ltd. (Shanghai, China). All solvents and chemicals were of analytical grade and used directly without further purification unless otherwise specified. Doubly purified deionized water (18.2 MΩ, Millipore, MA, USA) was used for the preparation of all aqueous solutions.

A cyclopore polycarbonate membrane, containing 2 μm diameter conical-shaped ordered micropores (Catalog No 7060-2511; Whatman, Maidstone, U.K.), was employed as the template. Platinum plating solution was consisted of 33 mmol/L H_2PtCl_6, 33 μmol/L $Pb(NO_3)_2$, and 0.5 mol/L HCl. Nickel plating solution was consisted of 84 mmol/L $NiCl_2{\cdot}6H_2O$, 1.6 mol/L $Ni(H_2NSO_3)_2{\cdot}4H_2O$, and 322 mmol/L H_3BO_3. The Pt–Ni mixture solution was prepared by mixing equal volumes of the platinum plating solution and nickel plating solution. The washing solution (PBST-20X) was consisted of 0.05 mmol/L phosphate buffer solution (PBS, pH 7.0), containing 0.15 mol/L potassium chloride and 0.05% Tween-20.

2.2 Fabrication of electrochemical cell device

An electrochemical cell was utilized for the deposition of electronic conductive polymer and metal materials into those micropores. The electrochemical cell was custom-built and designed by Teflon to resist chemical corrosion, similar to a reported procedure[20] with some modifications. **Fig**. **S1A** and **B** show the top view and lateral view photographs, respectively. As seen, the prepared cell could hold about 8 mL solutions. The principal aim of the cell is to hold the Pt-coated side of the membrane in place as working electrode in the electroplating solution along with the reference and counter electrodes. The dimensions were chosen to make full use of polycarbonate membrane while maximizing the surface area for plating. By electrochemically reducing metal ions Ni^{2+} and Pt^{4+} from the solution into the Pt-backed pores of the membrane template, microtubules could grow with thickness increase correspondingly to the increase of applied charges.

For the most part, the designed cell worked well in this system. The synthesis of magnetic imprinted micromotors proved to be reproducible, and a simple adjustment of either the current upper limit or polymerization time provided consistent results. A commercial polycarbonate membrane was used as the template, with a filtration pore structure of 2 μm in diameter on both sides and 20 μm in thickness. Such a polycarbonate membrane could provide an attractive template structure, as required for the bubbling propulsion mechanism.[21] SEM images of the front and back of polycarbonate membrane were shown in **Fig. S1C** and **D**. The polycarbonate membrane was sputtered with Pt layer on one of its back sides to provide the conductivity and thereby to be used as working electrode. The polycarbonate membrane after sputtered a conductive Pt layer was shown in **Fig. S1E** and **F**. So, all these photograph and image results proved that the membrane can be used as an ideal template in the template electrochemical deposition method.

2.3 Processing of polycarbonate membrane

The polycarbonate membrane was sputtered with Pt layer on dark side to provide the conductivity and was used as working electrode, and then it was put in 20 mL phycocyanin protein (0.5 mg/mL). After ultrasonic processing for 3 min to remove the air in the micropores, the membrane was incubated at 25 °C for 30 min. Electrostatic forces would drive the phycocyanin to filter into the space in the ordered micropores, and the pores surface of polycarbonate membrane were fully filled with the protein solution. The membrane was dried in air for 20 min. After sequentially rinsed with water, PBST-20X and water, the membrane was then assembled in a custom-built plating cell with an aluminum foil serving as a contact with the Pt layer. A Pt wire and an Ag/AgCl (3 mol/L KCl) were served as the counter and reference electrodes, respectively.

2.4 Preparation of tubular micromotors

Tubular micromotors were prepared by template electrochemical

deposition method following the process of five step electrodeposition protocol similar to a reported procedure[19,22] with necessary modification. Briefly, poly(3,4-ethylenedioxythiophene) (PEDOT) layers were firstly deposited potentiostatically for 574 s at +0.80 V using a charge of 4 C from a plating solution containing 10 mM EDOT and 125 mM NaPSS. Subsequently, an initial Pt layer was deposited galvanostatically at -2 mA for 200 s from a platinum plating solution to improve the mechanical properties of the polymeric layer. Then, an additional Pt–Ni layer was deposited galvanostatically at -2 mA for 300 s from a Pt–Ni mixture solution to provide a smooth and high conductive surface after the polymer deposition and improve the deposition of subsequent metallic layers. An intermediate Ni layer was then deposited potentiostatically at -1.3 V for 2.0 C from a Ni plating solution to provide magnetic guidance. Finally, the inner catalytic Pt layer was deposited galvanostatically at -2 mA for 450 s. The related parameters were listed in **Table S1**.

2.5 Preparation of magnetic imprinted microsensor

The deposited membrane was taken out from the electrochemical cell, and the sputtered Pt layer on the dark side of membrane was completely removed by hand polishing with a 3–4 μm alumina powder. The resulting PEDOT-Pt-Ni-Pt multilayer microtubes were released from the membrane by immersion in a dichloromethane solvent that also removes the template protein, leaving imprinted nanocavities on their micromotor outermost surface. After completely dissolving the membrane and removing the protein template, the magnetic imprinted micromotors were separated from membrane micropores. The micromotors were rinsed twice with dichloromethane, ethanol and ultrapure water, respectively, and were collected by centrifugation at 6000 rpm for 3 min. All magnetic imprinted micromotors were stored in ultrapure water at room temperature until use. As a control, magnetic non-imprinted polymer (NIP) micromotors were also prepared under identical conditions without phycocyanin molecules in the reaction system.

2.6 Characterization of magnetic imprinted microsensor

Ion sputter (E-1045, HITACHI) was used to spurt the polycarbonate membrane with platinum layer. The work conditions were performed at room temperature under base vacuum of 7.0 Pa, electric current of 15 mA and sputtering time of 200 s. The microscopic morphologies of magnetic imprinted micromotors were observed by scanning electron microscopy (SEM, JSM 5600 LV, 5kV). All samples were sputter-coated with gold before SEM analysis. Element analysis was carried out with energy dispersive X-ray (EDX) mapping analysis on scanning electron microscopy to confirm the multilayer content. A fluorescence microscope (BX61, Olympus) was employed to observe the fluorescence microscopy image of sample on a glass slide equipped with a CCD camera, 20X objective (unless mentioned otherwise) and acquired at a frame rate of 10 frames/s using the SPOT Advanced 4.6 software was used to capture fluorescence images. Further observations and videos were conducted and captured by using confocal laser scanning microscopy (CLSM) (FV1000, Olympus). The protein coverage on the micromotors was estimated to fluorescence qualitative analysis using the corresponding time-lapse images by the ImageJ software (where 100% means complete fluorescent coverage of the exposed surface). The average fluorescence-intensity values were obtained from triplicate independent results used for the following discussion.

2.7 Batch procedure of fluorescence protein recognition properties

To evaluate the protein recognition properties of the magnetic imprinted micromotors, adsorption time, phycocyanin concentration, sodium cholate and hydrogen peroxide concentration were investigated by a batch method. The procedures for phycocyanin concentration determination were carried out as follows. 50 μL of magnetic imprinted micromotors solutions were proceeded by removing the supernatant at 6000 rpm for 3 min, and equilibrated with 50 μL phycocyanin solutions with concentrations varying from 0.25 to 1 mg/mL in 0.05 mol/L phosphate buffer solutions (pH 7.0) for 30 min. The supernatants were removed by centrifugation, and then the micromotors were collected and re-suspended in 50 μL of phosphate buffer (0.05 mol/L, pH 7.0). 5 μL of a solution mixture was placed on a glass slide and observed by the fluorescence microscopy.

In order to determine the dependence of the surface coverage on the adsorption time, related experiments were conducted as below. 2 μL of magnetic imprinted micromotors solution equilibrated with 2 μL of 0.5 mg/mL phycocyanin was placed on a glass slide. It was observed by the fluorescence microscopy with 20X objective for 0, 5, 10, 15, 20, and 25 min, respectively, and then the fluorescence on the surface of the micromotor was captured by time-lapse photos. The corresponding photos were utilized to determine phycocyanin surface coverage on the micromotors with adsorption time change by the ImageJ software.

The capture and transport experiments were performed by using CLSM. The magnetic imprinted micromotor solution was consisted of four solutions, including 2 μL of magnetic imprinted micromotors, 2 μL of 3% sodium cholate, 2 μL of 3% H_2O_2 and 2 μL of phycocyanin (1 mg/mL) solution, which were successively added dropwise onto a glass slide. The fluorescence images of moving micromotors were collected and captured in video.

3. Results and discussion

3.1 Preparation and characterization of magnetic imprinted microsensor

The magnetic imprinted micromotor sensor was prepared by using modified template electrochemical deposition method,[19,22] as illustrated in **Fig. 1**. The procedure contained the processing of polycarbonate membrane (**Fig. 1A** and **B)**, five-step electrochemical deposition (**Fig. 1C**), and the construction of magnetic imprinted micromotor (**Fig. 1D** and **E**). The critical step for selective recognition and controllable self-propelled ability of microtubules is the five-step electrochemical deposition of various materials. The surface-imprinted PEDOT doped with PSS complex is ideal for imprinting of protein targets, because the matrix shows low nonspecific protein adsorption, and offers clear advantages in terms of controlling the deposition process and compatibility with aqueous media. The outer tubular PEDOT layer of micromotors was grown on the inner walls of the polycarbonate membrane micropores, which contained the pre-adsorbed phycocyanin molecules. The outer layer was formed by

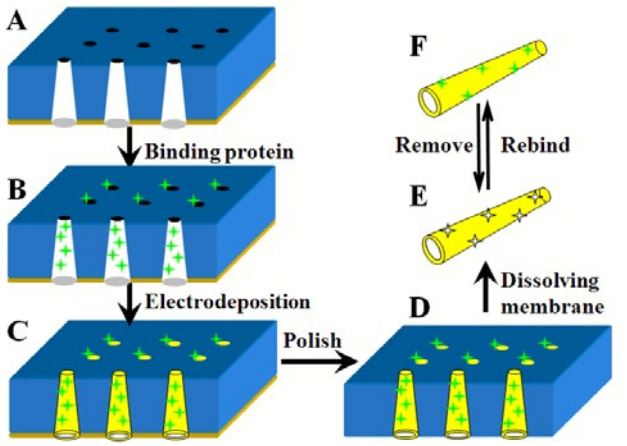

Fig. 1 Scheme illustration for the preparation process of the magnetic imprinted microsensor. (A) Sputtering a conductive Pt layer on polycarbonate membrane, (B) polycarbonate membrane adsorbs the negatively charged protein by electrostatic interaction, (C) sequential deposition is used to deposit the PEDOT/PSS, inner Pt, Pt–Ni, Ni and Pt layers, (D) conductive Pt layer is completely removed by hand polishing, (E) the resulting PEDOT-Pt-Ni-Pt multilayer microtubules are released from the membrane by immersion in dichloromethane as well as the template proteins are removed, and (F) magnetic imprinted micromotors adsorb template protein.

sequential electrodeposition of the inner Pt, Pt–Ni, Ni and Pt metallic layers. Among them, Ni was used for magnetic guidance; Pt was used as micromotor skeleton and catalyst to produce the oxygen-bubble to supply propulsion power. Then the sputtered conductive Pt layer on the dark side of membrane was completely removed by hand polishing. Finally, the magnetic imprinted micromotor sensor was obtained by dissolving the membrane and removing the protein template molecules (**Fig. 1E**). The microsensor with specific cavities could specifically and easily interact with the phycocyanin molecule through hydrogen bonds and electrostatic interactions (**Fig. 1F**).

SEM images of the typical conical micromotor sensor were displayed in **Fig. 2.** As seen the side-view (A, B) and cross-view (C), the MIP-based microsensor had a defined geometry with two-end outer diameters of 1.8 and 1.0 μm, along with inner openings of 1.5 and 0.7 μm, and a total length of 18 μm. The MIP microsensor exhibited a highly rough outside polymeric surface (**Fig. 2C**), reflecting a large number of exposed complementary imprinted cavities on the surface of the micromotor. In contrast, a much smoother surface was observed on the NIP micromotor (**Fig. 2D**). The difference proved that MIP-based micromotor possessed much larger specific area than that of the corresponding NIP one, suggesting more additional binding sites were produced by eluting the template molecules of MIPs. Meanwhile, the essential conical shape of the micromotor was retained following the imprinting process.

EDX mapping analysis was carried out to confirm the electrodeposition materials, as recorded in **Table S2**. All the plating solutions could be electroplated into the shell of the micromotor, thickness of which was increased by increasing charge. Continuous transformation of plating solutions of different metal ions with one another allowed one to deliberately and systematically prepare multilayer microtubules. The presence of both oxygen (27.0%) and carbon (46.7%) was from organic materials PEDOT/PSS, Ni (0.55%) and Pt (24.55%) were

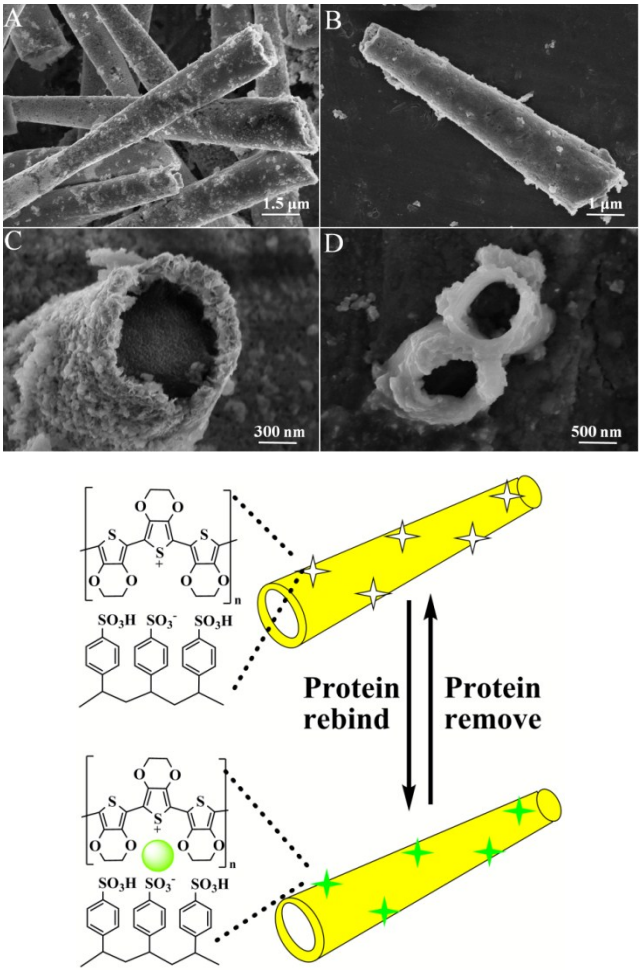

Fig. 2 (Upper) SEM images of magnetic (A–C) MIP micromotor and (D) NIP micromotor. (Below) Scheme of magnetic MIP micromotor rebinds and removes protein.

electrochemically reduced from the plating solution into the conical microtubules, and Pb (0.40%) as a modifier of platinum plating solution was found as well. These experimental data in **Table S2** were able to provide direct evidence for the successful growth of the multilayer micromotor. Therefore, a magnetic imprinted micromotor sensor was successfully obtained based on template electrochemical deposition method.

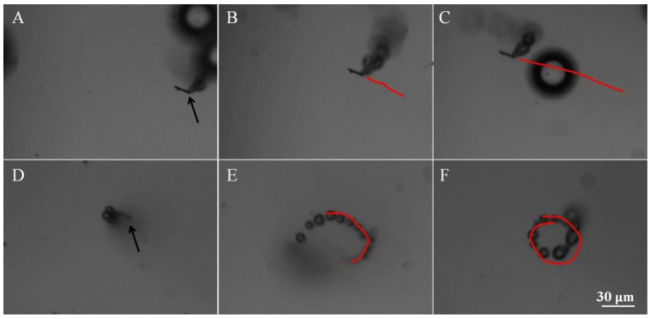

Fig. 3 Motion images of the micromotor propel in the solution with (A–C) straight and (D–F) spiral motion trajectories. Red traces denote the path travelled by the micromotor

3.2 Optimization of motion control conditions of the microsensor

The major influential factors on motion conditions of the micromotors generally include surfactant, H_2O_2 concentration, magnetic field, and micromotor shape.[23,24] In this work, the micromotor shape was determined by the membrane template, which had been fixed; according to preliminary experimental results, 1% H_2O_2 was used. So, herein, surfactant and magnetic field were carefully taken into account to achieve the optimal conditions for desired motion trajectories.

The surfactant effect was examined for the motion of micromotor in 1% H_2O_2. Due to the high surface tension of water, the produced O_2 bubbles were usually big in water, which neither was in favour of the observation of the microtubules movement status, nor facilitated the diffusion of fresh H_2O_2 solution into the interior of the microtubules. So, herein, sodium cholate surfactant was used to control the diameters of the oxygen bubbles produced in H_2O_2 solution, and to promote the exchange of H_2O_2 solution both inside and outside the microtubules, and thereby to replenish fresh H_2O_2 solution into microtubules to speed up the movement of microtubules. The surfactant effect upon the oxygen bubbles was investigated. As seen in **Fig. S2A–C**, the oxygen bubbles diameter reduced from more than 150 to 20 μm upon with the surfactant concentrations increasing. When the concentration of sodium cholate exceeded a fixed value, the size of the bubbles would not reduce any more (**Fig. S2D**), and then it was decided by the structure of the microtubules. Finally, the most favourable surface morphology and motion trajectories were obtained by using 1% H_2O_2 in the presence of proper sodium cholate at 2%.

As seen, **Fig. 3** and SI Video 1 illustrate the obtained motion trajectories of the high propulsion power magnetic imprinted micromotor. The micromotor showed two types of motion trajectories: one was straight trajectory with long oxygen bubble tails, which were released from the wider tubular openings, as shown in **Fig. 3A–C**; the other was spiral and circular trajectory, with a high average speed of 113 μm/s, as shown in **Fig. 3D–F**. The micromotor exhibited various motions trajectories depending on the distribution of the platinum inside the tubes, as displayed in SI Video 1. The mechanism responsible for these motions can be explained by the assumptions that spatial unbalance of force or torque affects motion trajectories.[25] The propulsion force was controlled by catalytic activity of platinum amount, and constant force/torque would be produced in the same manner as in composite motors. For example, when the platinum in the internal distribution of microtubule was not uniform, and thereby resulted in the rate of bubble produced uneven in different places, the micromotor would exhibit circular, spin, and rotation motions, respectively. If the platinum showed uniform distribution in the interior of the microtubules, it would move in straight trajectories.

Then, in the above optimized solutions, magnetic field effect was investigated. SI Video 2 shows time-lapse images of the micromotor motion under a magnetic field in the presence of 1% H_2O_2 and 2% sodium cholate. As seen from the video, while the imprinted micromotor moved randomly, it was also possible to guide them magnetically by the intermediate ferromagnetic Ni layer. The micromotor moved rapidly in straight trajectory at first, and then it moved in a curved trajectory after a magnet was placed on one side of the micromotor (SI Video 2). So, the imprinted micromotor sensor was demonstrated to be capable of directional motion effectively guided by magnetic fields.

3.3 Motion mechanism of the microsensor

To figure out what the motion velocity of the micromotor sensor depended on, it was required to quantitatively determine the bubble generation frequency and the average moving step length caused by the bubble ejection. The mechanism may be inferred that the bubble expelling frequency depended upon the production rate of oxygen (O_2) and the bubble size, which was applicable to the present two types of motion trajectories. The production rate could be determined experimentally by measuring the volume of the produced O_2 from a planar Pt surface with predefined area.

The experimental results indicated that the productivity of O_2 could be linearly proportional to the area of Pt surface and the H_2O_2 concentration C_{H2O2}. The average velocity of the micromotor moving in the H_2O_2 solution, v_m, could be expressed referring to that reported as follows[21]:

$$v_m = f \times l = \frac{9nC_{H_2O_2}R_mL}{3R_b^2 + LR_b/(\ln(\frac{2L}{R_m}) - 0.72)} \quad (1)$$

where, f is defined as the bubble generation frequency, l is the average moving step length, n is O_2 rate constant, C_{H2O2} means the H_2O_2 concentration, L is the micromotor length, R_m is the radius of the tubular cavity, and R_b indicates the average radius of bubble.

According to Eqn. (1), it could predict that the average micromotor velocity υ_m was linearly proportional to C_{H2O2} and also depended upon the micromotor length L and micromotor radius R_m. Also, the catalytic motion of micromotors in the H_2O_2 solution was indicated to be complex, and the velocity was influenced by a number of experimental parameters, especially the micromotor geometry and the chemical environment.

Furthermore, under the present conditions, n could be experimentally estimated to be 9.8×10^{-4} m/s from both flat and rolled surfaces in H_2O_2 with concentrations up to 10%. And the micromotor length L could be 18 μm, the radius of the tubular cavity R_m could be 1.5 μm, the equivalent bubble radius R_b should be larger than the radius of the microjet R_j. And when the H_2O_2 concentration C_{H2O2} was below than 3% in the experiments, the results could well fit with the relationship of R_b = 1.2 R_m. Hence, Eqn. (1) could also be simplified as follows:

$$v_m = 1.04 \times 10^{-2} C_{H_2O_2} \quad (2)$$

As seen from Eqn. (2), the H_2O_2 concentration could strongly influence the velocity of the catalytic micromotors. Our further experimental results showed that the average moving speed of the micromotor increased from 113 μm/s at 1% H_2O_2 to 163 μm/s at 1.5% H_2O_2, as illustrated in SI Video 3. Correspondingly, it could be calculated according to Equ. (2) that the moving speed increased from 104 to 156 μm/s, respectively. Good fitting between experimental and calculated results proved the validity

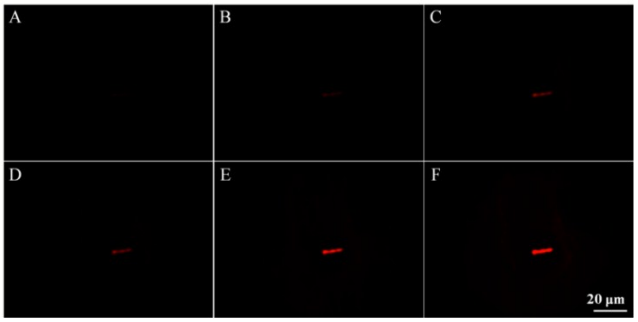

Fig. 4 Fluorescence microscope photos of the magnetic imprinted micromotor propel in the phycocyanin protein solution during the different time periods for (A) 0, (B) 5, (C) 10, (D) 15, (E) 20, and (F) 25 min. Experimental condition: time-lapse images each taken over a 5 s period; phycocyanin protein solution concentration was 0.5 mg/mL.

of the equations. Therefore, it could be concluded that the body-deformation model[26] was considered to be satisfactory and feasible.

3.4 Binding properties of the magnetic imprinted microsensor

Based on the above studies, such motion based isolation routes could enable direct visualization of the binding events based on the movement of the micromotor sensor. The existence of phycocyanin binding sites on the outside surface of the microsensor was confirmed by adsorption isotherm experiments, and the binding properties were investigated as follows.

The micromotor was incubated in 0.5 mg/mL phycocyanin solutions over time. The imprinted polymeric layer was capable of selectively capturing the fluorescent target protein onto the micromotor, and then the micromotor could emit red fluorescence under UV light observed by fluorescence microscope. Such capture was illustrated in **Fig. 4A–F**, which showed the influence of time upon the adsorption capacity, estimated from the fluorescence coverage. The time-lapse images illustrated that the surface coverage had relatively low initial adsorption rates and then linearly increasing rates with time up to 20 min (**Fig. 4A−E**). It was observed that complete fluorescent coverage was approached within 25 min (**Fig. 4F**), and the adsorption kinetics proved favourable and rapid.

This phenomenon could be explained as follows: by combining surface imprinting with PEDOT/PSS, most recognition sites were situated on the outside surface of the micromotor, which facilitated the mass transfer and capturing. Therefore, the formation of surface-imprinted micromotor was highly desirable to improve the binding capacity, as well as enable the equilibrium to be achieved within a shorter period of time. **Fig. S3** indicates that a short time (20 min) offered convenient isolation of the target protein. Therefore, the concentration dependence of the magnetic imprinted micromotor for protein interaction was evaluated by using a time of 20 min.

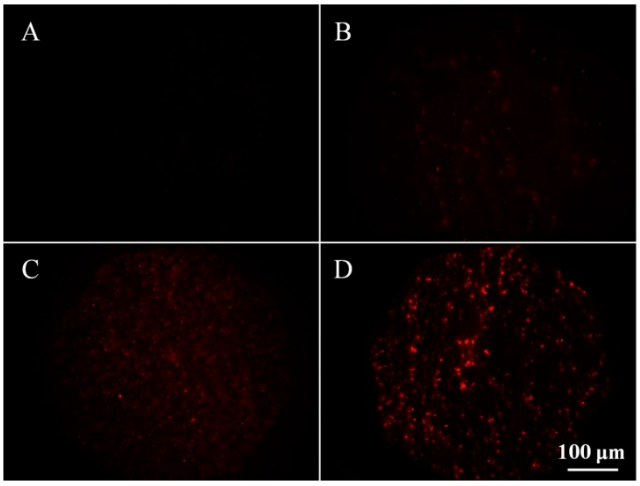

Fig. 5 Fluorescence microscope photos of the magnetic imprinted micromotor for 20 min in a solution containing increasing concentrations of phycocyanin target protein: (A) 0, (B) 0.5, (C) 0.75, and (D) 1 mg/mL.

The adsorption isotherm experiments for the micromotor sensor were carried out in various concentrations phycocyanin solutions for 20 min incubation, ranging from 0−1 mg/mL, and then thoroughly washed, and imaged by fluorescent microscope. **Fig. 5A–D** display images of the magnetic imprinted micromotor sensor along with the increasing initial concentrations. A gradual increase in the fluorescence intensity was observed as the phycocyanin concentration increased. As seen in **Fig. S4**, The corresponding plot of fluorescence intensity versus concentration showed a nearly linear dependence up to 0.75 mg/mL phycocyanin. At equilibrium concentrations higher than 1.0 mg/mL, adsorption of the micromotor became stable and its recognition sites were almost saturated. The fluorescence intensity could thus provide a rough quantitative estimation of the protein concentration.

So, the resulting magnetic imprinted micromotor sensor offered direct recognition, capture, and transport, and the fluorescent target protein provided real-time optical visualization images of the MIP binding event based on changes in the fluorescence intensity. Furthermore, specific binding is a key requirement for the new MIP-based microsensor isolation platform. Thus, controls experiments were required to evaluate the binding specificity of the phycocyanin-imprinted microsensor toward phycocyanin, as seen in **Fig. S5**. The NIP PEDOT/PSS microsensor did not emit apparent fluorescence (**Fig. S5B**), suggesting that the microsensor could not bind the template protein, despite it was soaked in the higher concentration phycocyanin solution for a long time. As well, the phycocyanin-imprinted microsensor showed no fluorescence after soaking for 20 min in a solution containing the protein BSA (**Fig. S5C**). At the same time, through ultraviolet absorption spectra, the BSA concentration still showed no obvious change before and after soaked in the solution. Therefore, the specificity of the MIP−PEDOT/PSS microsensor was clearly demonstrated, showing the crucial role of the MIP recognition sites in attaining such efficient and selective uptake of the target protein, and the negligible nonspecific adsorption onto the PEDOT/PSS outer polymer.

Moreover, due to the highly cross-linked polymeric and

deposited metal nature, the MIP microsensor showed good physical stability and chemical inertness. Further analysis and regeneration of the microsensor could be accomplished by elution using a regeneration solution to take off rebinding protein followed by rinsing with a neutral PBS to restore the neutral blank status. Such elution did not compromise the movement and combining ability of the microsensor. Furthermore, the microsensor was indicated excellently reproducible due to the recoverability of 5 cycles with the standard error within 10%, As for the long time stability, the MIP microsensor had been shown to be stable even 90 days after their preparation when it was stored at 4 °C in a refrigerator.

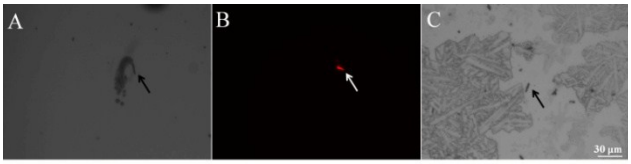

Fig. 6 (A) Microscope photo of the magnetic imprinted micromotor in seawater with target phycocyanin protein; (B) fluorescence time-lapse photo taken after the micromotor moved in seawater with phycocyanin for 20 min; (C) microscope photo of the micromotor after evaporation of the solution.

3.5 Applications of the microsensor to seawater samples

In order to evaluate the practical utility of the developed MIP microsensor for phycocyanin recognition and transport, unprocessed natural seawater samples were applied for further investigation. As shown in **Fig. 6A**, the efficient propulsion of the MIP microsensor in the seawater samples at speeds of 78.8 ± 2.9 μm/s allowed their prolonged movement and direct isolation of the phycocyanin without tedious sample processing steps. The change in the speed (usually higher than 100 μm/s above mentioned) could be ascribed to the viscosities and matrix effects of seawater, and the adsorption of molecules onto the catalytic Pt layer. **Fig. 6B** clearly illustrates the effective accumulation of the target phycocyanin onto the microsensor from phycocyanin-spiked seawater samples during 20 min interaction. Such efficient binding was not compromised by the presence of a large excess of coexisting ions in the seawater samples. As seen from **Fig. 6C**, after evaporation, a large number of seawater salinity was left on the glass surface, and fortunately, it did not affect the phycocyanin adsorption in the microsensor. Overall, **Fig. 6** supported the high specific enrichment ability of the MIP based microsensor, and confirmed its feasibility for isolation and transport of the target protein in complex samples.

In the complex seawater matrices, the target phycocyanin recognition should be coupled with effective discrimination against coexisting compounds and salts. Because the fluorescence intensity of micromotor outside surface was weak, the fluorescence on the surface of the micromotor was required to be captured by time-lapse photos, and therefore it could not directly take video of the moving fluoresce micromotor. So, in order to get video, the fluorescent phycocyanin protein was added into the solution to produce fluorescence, while the bubbles induced by the micromotor had no fluorescence, and thereby through a contrast, real-time video could be taken. As recorded in SI Video 4, the phycocyanin adsorption did not interfere with the efficient bubble propulsion. The video results further indicated the MIP micromotor sensor could realize real-time visualization imaging in complex samples, along with effective propulsion and recognition/capture of phycocyanin. Consequently, algae bloom monitoring and removal could be performed since phycocyanin is often used as the index of cyanobacteria.

4. Conclusions

In summary, a simple and rapid magnetic imprinted micromotor sensor with high selectivity and sensitivity was developed by combining MIPs and catalytic microtubule, based on porous PEDOT/PSS template assisted sequential electrodeposition protocol, and was successfully applied to effective label-free fluorescent phycocyanin recognition and transport. By taking full advantages of the custom-tailored MIPs, as well as the catalytic, magnetic and electrochemical responsive properties, the obtained microsensor easily realized the specific identification, autonomous adsorption/enrichment, and controllable motion of phycocyanin, even targeted directional transport and isolation from seawater matrices. The present phycocyanin imprinted microsensor opens promising prospects for the development of MIPs-based platforms for the selective isolation and sensitive sensing of various target analytes coupled with the construction of self-propelled micro/nanoscopic objects. Such studies will greatly contribute to marine pollution monitoring and abatement, extend the research connotations of concerned-targets imprinting, as well as push forwards the development of intelligent micro/nano-scale apparatus and strategies.

Acknowledgments

This work was financially supported by the National Natural Science Foundation of China (21275158, 21477160), the Strategic Priority Research Program of the Chinese Academy of Sciences (XDA11020405), the Innovation Projects of the Chinese Academy of Sciences (KZCX2-EW-206), and the Scientific Research Foundation for the Returned Overseas Chinese Scholars, State Education Ministry.

Notes and references

[a] *Key Laboratory of Coastal Environmental Processes and Ecological Remediation, Shandong Provincial Key Laboratory of Coastal Environmental Processes, Yantai Institute of Coastal Zone Research, Chinese Academy of Sciences, Yantai 264003, China*

[b] *University of Chinese Academy of Sciences, Beijing 100049, China*

** Corresponding author. Fax: +86 535 2109130 , Tel: +86 535 2109130. E-mail: lxchen@yic.ac.cn;*

† Electronic supplementary information (ESI) available. See DOI: 10.1039/b000000x

1 X. Chuai, W. Ding, X. Chen, X. Wang, A. Miao, B. Xi, L. He and L. Yang, *Ecol. Eng*., 2011, **37**, 842–849.

2 M. Gantar, D. Simović, S. Djilas, W. W. Gonzalez and J. Miksovska, *J. Biotechnol.*, 2012, **159**, 21–26.

3 J. N. Boyer, C. R. Kelble, P. B. Ortner, and D. T. Rudnick, *Ecol. Indic*., 2009, **9**, 1188–1197.
4 K. Song, L. Li, Z. Li, L. Tedesco, B. Hall and K. Shi, *Ecol. Inf*., 2013, **15**, 22–33.
5 K. Song, L. Li, L. Tedesco, S. Li, B. Hall and J. Du, *ISPRS J. Photogramm. Remote Sens*., 2014, **95**, 68–80.
6 N. T. Eriksen, *Appl. Microbiol. Biot*., 2008, **80**, 1–14.
7 Z. Zhang, L. Chen, F. Yang and J. Li, *RSC Adv*., 2014, **4**, 31507–31514.
8 L. Chen, S. Xu and J. Li, *Chem. Soc. Rev*., 2011, **40**, 2922–2942.
9 J. Li, Z. Zhang, S. Xu, L. Chen, N. Zhou, H. Xiong and H. Peng, *J. Mater. Chem.*, 2011, **21**, 19267–19274.
10 H. Liu, G. Fang and S. Wang, *Biosens. Bioelectron*, 2014, **55**, 127–132.
11 M. J. Whitcombe, I. Chianella and L. Larcombe, *Chem. Soc.Rev*., 2011, **40**, 1547–1571.
12 C. S. Mahon and D. A. Fulton, *Chem. Sci*., 2013, **4**, 3661–3666.
13 S. Wang, J. Ye, Z. Bie and Z. Liu, *Chem. Sci.*, 2014, **5**, 1135–1140.
14 Z. Zhang, J. Li, J. Fu and L. Chen, *RSC Adv*., 2014, **4**, 20677–20685.
15 D. Kagan, S. Campuzano, S. Balasubramanian, F. Kuralay, G. U. Flechsig and J. Wang, *Nano Lett*., 2011, **11**, 2083–2087.
16 V. Garcia-Gradilla, J. Orozco, S. Sattayasamitsathit, F. Soto, F. Kuralay, A. Pourazary, A. Katzenberg, W. Gao, Y. Shen and J. Wang, *ACS nano*, 2013, **7**, 9232–9240.
17 J. Wang and W. Gao, *ACS nano*, 2012, **6**, 5745–5751.
18 G. Huang, J. Wang and Y. Mei, *J. Mater. Chem*., 2012, **22**, 6519–6525.
19 J. Orozco, A. Cortés, G. Cheng, S. Sattayasamitsathit, W. Gao, X. Feng, Y. Shen and J. Wang, *J. Am. Chem. Soc*., 2013, **135**, 5336–5339.
20 M. J. Banholzer, L. Qin, J. E. Millstone, K. D. Osberg and C. A. Mirkin, *Nat. protoc*., 2009. **4**, 838–848.
21 J. Li, G. Huang, M. Ye, M. Li, R. Liu, Y. Mei, *Nanoscale*, 2011, **3**, 5083–5089.
22 W. Gao, S. Sattayasamitsathit, A. Uygun, A. Pei, A. Ponedal and J. Wang, *Nanoscale*, 2012, **4**, 2447–2453.
23 W. Gao, A. Pei, X. Feng, C. Hennessy and J. Wang, *J. Am. Chem. Soc*., 2013, **135**, 998–1001.
24 M. Manjare, B. Yang and Y. Zhao, *J. Phys. Chem. C*, 2013, **117**, 4657–4665.
25 D. Yamamoto, A. Mukai, N. Okita, K. Yoshikawa and A. Shioi, *J. Chem. Phys*., 2013, **139**, 034705.
26 M. García, J. Orozco, M. Guix, W. Gao, S. Sattayasamitsathit, A. Escarpa, A. Merkoçi and J. Wang, *Nanoscale*, 2013, **5**, 1325–1331.